SSRG International Journal of Mechanical Engineering
ISSN: 2348-8360/ https://doi.org/10.14445/23488360/IJME-V13I7P115

Volume 13 Issue 7, 174-187, July 2026
© 2026 Seventh Sense Research Group®

Original Article

Investigation of the Aerodynamic Characteristics of a Morphing Airfoil for Unmanned Aerial Vehicles

Anmar H. Ali[1], Basim A. R. Al-Bakri[2]

[1]*Department of Aeronautical Engineering, University of Baghdad, College of Engineering, Baghdad, Iraq.*
[2]*Aeronautical Engineering Department, University of Baghdad, College of Engineering, Baghdad, Iraq.*

[1]*Corresponding Author : anmar.h.a@coeng.uobaghdad.edu.iq*

Received: 05 May 2026 Revised: 23 June 2026 Accepted: 13 July 2026 Published: 30 July 2026

Abstract *- An effective method for improving the aerodynamic efficiency of flight is the use of morphing technology. This technique is currently used in many applications for controlling existing UAVs. A new proposal of NACA 2415 airfoil internal structure was capable of changing the camber line with Rectangular Corrugated Variable Camber (RCVC), which was used and analyzed aerodynamically by evaluating the pressure, lift, drag, and lift-to-drag coefficients. The curvature geometry of the airfoil was represented by a simple recurved system mathematical model and programmed using MATLAB. The airfoil was 3D printed using PLA material and compared with the recurved system model for matching with good accuracy at positive and negative deflection angles. The numerical solution by Xflr5 version 6 software (viscous-inviscid method) and by a computational fluid dynamics solution using the EasyCFD program were used to calculate the aerodynamic performance of the airfoil. The Reynolds number (Re) is 0.688 x 10^6, while angles ranging from 0 ° to 20 ° were used as flap angles and also angles of attack for morphing, flapped airfoil, and the normal one, respectively. The results were compared between the morphed airfoil and the conventional deflected flap airfoil, where the flap chord is 40% of the airfoil's length, has been evaluated. The lift and drag coefficients, lift-to-drag ratio, and pressure distribution on the airfoil surfaces were discussed and compared with published experiments. The results show that the morphing airfoil, with an increasing aerodynamic efficiency to 28%.*

Keywords *- Variable Camber Airfoil, Aerodynamic Characteristics, Corrugated Airfoil Structure, Adaptive Airfoil.*

1. Introduction

Improving UAV performance is crucial to increasing manoeuvrability and reducing energy consumption. Aerodynamic surfaces are rigid, segmented, and discrete structures that can move relatively to alter their aerodynamic coefficients. The conventional fixed airfoils for a wide range of operating envelopes of UAVs cannot give the optimum aerodynamic performance because a single airfoil geometry may have difficulty simultaneously satisfying the aerodynamic requirements of takeoff, climb, cruise, and maneuvering flight. These surfaces can operate within a specific range and under certain conditions. Beyond this range, these technologies negatively impact aerodynamics, resulting in reduced performance. As an example, the conventional rigid airfoils, NACA 2415, are optimized for a narrow, fixed operational envelope. The maximum lift-to-drag ratio for this airfoil is 45-50 at design cruise $\alpha = 4$. Off-design conditions, such as high-lift takeoff and landing or high-speed loitering, lead to a drop in the aerodynamic performance of about 25%-35%, because the geometry cannot adapt to optimize the pressure distribution. Aerodynamic optimization in multiple flight regimes by using a morphing technique that enhances the usability of Unmanned Aerial Vehicles (UAVs). These enhancements are found in the range, endurance, and lift-to-drag ratio, especially at low to moderate Reynolds numbers. Morphing airfoils can change their shape in flight. This offers numerous advantages, including improved performance by adjusting the airfoil's shape to suit flight conditions and reducing structural weight by eliminating the complex mechanisms used to move ailerons and flaps. In recent years, interest has focused on morphing wings, including those used in UAVs, to allow changes in one or more geometric parameters, such as chord length, maximum thickness, and camber.

Different morphing concepts have been studied over the years and summarized in several review works. A morphing wing with a compliant mechanism structure and an elastic skin that improves control surfaces and increases aerodynamic efficiency during steady flow at a Re= $0.3\text{x}10^6$ had been considered by [1]. The results are compared with conventional designs in terms of lift, drag coefficients, and pressure distribution. Using the CST (Class-shape Transformation) method and the XFOIL program for aerodynamic performance, a set of optimized airfoil shapes was generated that minimizes drag while achieving the required lift. A drag reduction of approximately 20-60% was achieved for the morphing airfoil compared to a conventional airfoil with a hinged flap.

A carbon fiber composite was proposed to make a morphing airfoil by [2]. The morphing camber can be fully controlled with multiple degrees of freedom using a Linear Ultrasonic Motor Actuation System (LUSM). Through numerical calculations and experimental results, the morphing airfoil demonstrated a high lift-to-drag ratio efficiency over a wide range of angles of attack. The compliant structure showed its ability to satisfactorily withstand loads and change its shape according to different morphing conditions.

The double-corrugated variable-camber morphing wings with aerodynamic and structural analysis for UAVs were studied by [3], utilizing the XFoil thin-wing theory program and the Finite Element Method (FEM) for structural analysis. The results show that the shape achieves a high lift-to-drag ratio and a high capacity to withstand high failure stresses while maintaining flexibility when bending, compared to the results of the FishBAC shape and single corrugated variable camber.

A complete structure with a morphing wing was manufactured for a 2-m-long fixed-wing carbon fiber composite UAV by [4]. A continuous 3D printing system for these fibers was developed by 9T Lab, designed using a distributed Additive Manufacturing method (AM). The UAV can be fully controlled in all directions without the need for conventional hinges, with a morphing wing trailing edge deflection of up to 48 mm. It was found that the distributed Additive Manufacturing (AM) method for printed fibers increases the load-bearing capacity and durability of the UAV's internal structure. This method is ideal, waste-free, and low-cost compared to conventional drone manufacturing methods. High roll rates of up to 240 deg/s have been demonstrated, making it possible to expand the scope of application to include small manned aircraft. Moulton et al. [5] demonstrate a rapid and feasible approach using low-cost 3D printing for UAVs, eliminating the complex assembly of most of the aircraft's parts. Two control methods for 3D-printed morphing wings are discussed. The first is the Airfoil Recambering Compliance System (ARCS), which is used for continuous-edge morphing wings. The second is the Kinematic Internal Nexus Compliance System (KINCS) for discontinuous trailing-edge wings. Both methods employ additive manufacturing based on fused deposition modeling, which is cost-effective and easy to manufacture. The second method is more efficient, as it is manufactured from a mono-material and produces a 25° deflection on the trailing edge of the wing. The research focuses on the mechanisms of multi-material 3D printing and on improving the flexibility and stiffness of the materials to resist structural failure.

A Single, Corrugated, Variable-Camber (SCVC) morphing airfoil model was used by [6], and the deformed beam theory was applied for structural analysis through a finite element method program. Two methods were used for the aerodynamic analysis: CFD and XFoil. The results show that the morphing improves the aerodynamic efficiency and load-bearing capacity under medium to high lift conditions at Re = $1x10^6$. The study highlights the benefits of morphing and the importance of determining the optimal morphing angle during different flight phases. A wing section airfoil model with a morphing trailing edge was designed and tested in a wind tunnel [7]. Using 3D printing, the model was fabricated in great detail using various materials for testing. Simultaneously, numerical calculations were performed to determine the aerodynamic characteristics, specifically studying the elastic deformation of the variable trailing edge. The study achieved a lift of 37.9 ° at an airspeed of 15 m/s. The results were verified by comparing the numerical and experimental data, revealing a 13% increase in lift.

High-efficiency design can be applied to drones under diverse operating conditions, as used by [8]. The continuously changing upper and lower wing surfaces allow for the generation of a variety of wing shapes with different thicknesses and curvatures. Improvements in wing performance at low Reynolds number $0.05x10^6$ were demonstrated through flow calculations, showing a 20% increase in both lift and lift-to-drag ratio. The fishbone wing design provides two control points for changing the wing shape. This work can serve as a basis for further research to improve aerodynamic performance.

Aerodynamic performance is improved through a morphing wing shape change technique [9]. The focus is on a Shape Memory Alloy (SMA) wire and a corrugated structure as an alternative to the hinged flaps used in an airfoil. This design is used to create a smooth morphing camber and a large deflection area in the trailing edge of the airfoil. This technique was applied to the Eppler E397 airfoil, with a morphing starting at 65% of the chord. This allows sufficient and smooth deflection. The finite element method was used to determine the wire position and length. The wing was tested using the vortex lattice method for its aerodynamic performance. Although numerous studies have investigated morphing airfoils for improving aerodynamic efficiency, most existing research has primarily focused on conventional fixed-wing configurations or has evaluated morphing mechanisms under limited flight conditions.

A review of previous research revealed that most of the structures used lack detailed manufacturing specifications or information on how to move and connect them to drive motors. Furthermore, they often involve kinetic mechanisms and manufacturing materials that can be costly. Therefore, the main objective of the current study in this article is to find the aerodynamic performance of a new, simple and easy manufacturing design morphing wing section NACA 2415 model that focuses on the use of the variable airfoil camber by the rectangular corrugation spaces, which can be called Rectangular Corrugated Variable Camber (RCVC). Unlike previous studies that mainly focused on conventional morphing concepts, the novelty of the present geometry of structure is the type of divisions that it increases the model's flexibility and ability to withstand forces due to the large external contact surface with the airfoil surface and provide smooth curvature of the morphing wing in both directions, reaching 40°-60° and enhance its aerodynamic performance. The aerodynamic analysis of various configurations will be performed using the EasyCFD program, and Xflr5 version 6 [10, 11], and comparisons will be made to determine the most feasible configuration. The following aspects will be addressed;

- Making a mathematical model to represent the new morphing geometry of the airfoil NACA 2415.
- 3D printing the geometry using PLA material with a specified accuracy and matching the tilting angles of the airfoil.
- Calculate its aerodynamic characteristics using Xflar5 v6 and a more-fidelity EasyCFD program to analyze the results.
- Compare the aerodynamic characteristics of the baseline and morphing airfoil configurations.
- Quantify the effects of airfoil morphing on lift coefficient, drag coefficient, lift-to-drag ratio, and pressure distribution.

Figure 1 illustrates the complete methodology of the current research, demonstrated using the flowchart method.

Fig. 1 The methodology flow chart

2. Geometry

A new design of a morphing airfoil of Rectangular Corrugated Variable Camber (RCVC), which provides an alternative design for inducing changes in airfoil curvature in both directions. The NACA 2415 wing section was used as the baseline for the wing model. A solid portion of the section was formed as the main D-beam, representing 31% of the airfoil section chord length, measured from the front of the section, while the curvature to the trailing edge is at 85% of the chord length, measured from the front of the section. The structure consists of dividing the wing section into appropriate sections, sized to match the required curvatures on the chord, distributed along the chord. These sections are connected in a manner compatible with the NACA 2415 shell, alternating upper and lower surfaces in the chord direction. These sections are bonded by a pre-tensioned Elastic Matrix Composite (EMC) outer surface. The wing section is partitioned using a cosine function, with the sections condensed near the trailing edge and coarse sections at the midpoint. This partitioning allows for greater curvature of the sections at the trailing edge than at the midpoint, as shown in Figure 2.

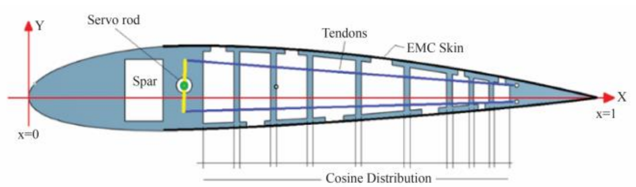

Fig. 2 Morphing airfoil section NACA 2415 composed of Rectangular corrugated with variable camber

As shown in Figure 2, to create a smooth, continuous curvature, a pair of strong, opposing tendons or connectors is installed. Their function is to generate equal and opposite displacements of the strings, generating a bending moment on the rigid trailing edge strip, which induces the trailing edge structure to bend, resulting in significant changes in the curvature of the wing. Further clarification can be seen in Figure 3, which shows the most important parts through which the wing is assembled and moved (spar, servo, connectors, pins, etc..)

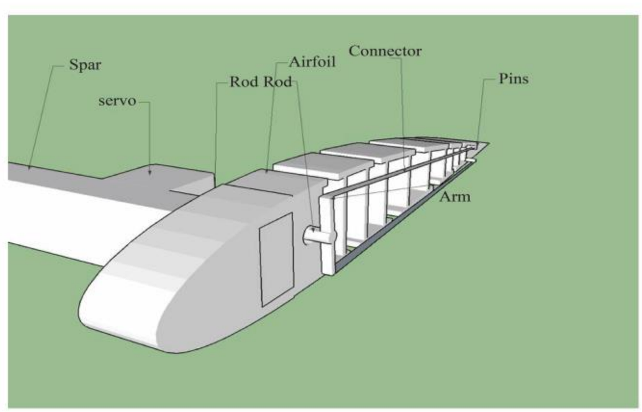

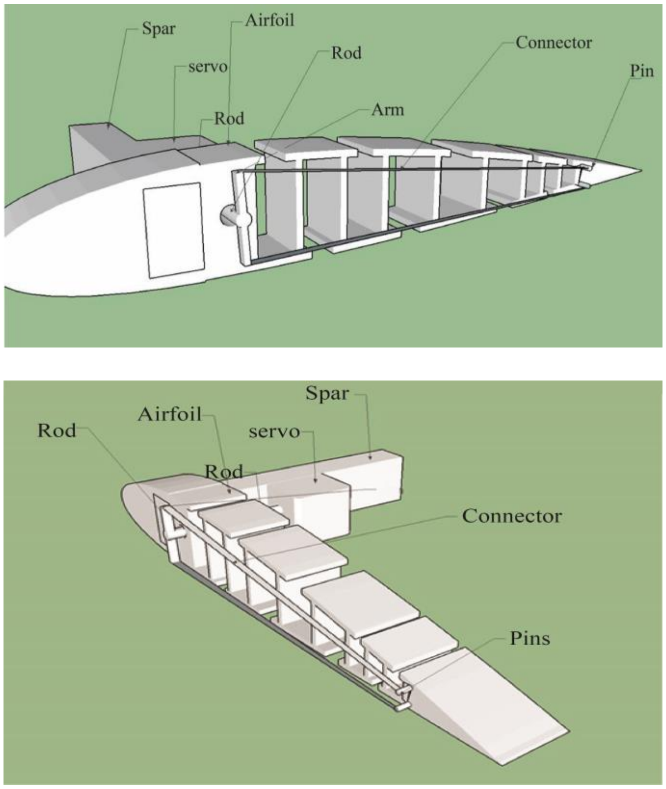

Fig. 3 A 3D view of a rectangular corrugated with variable camber airfoil structure

Table 1 shows the parameters of the printed airfoil that is used in the present consideration.

Table 1. Airfoil geometry

Airfoil parameters	Dimensions
Airfoil Type	NACA 2415
Chord Length	200 mm
Start morphing distance from L.E.	62 mm
End morphing distance from L.E.	170 mm
Thickness of divisions	5 mm
Tendon diameter	0.7 mm
Skin thickness (EMC)	2 mm

A servo connector was used to create the forming section, activated from both sides, as shown in Figure 3. The formed wing was drawn using CAD software in preparation for 3D printing. Polylactic Acid (PLA), a high-modulus polymer found in renewable resources, will be used to print the formed wing. It is important to fabricate the model with lightweight materials. Figure 4 shows the formed airfoil in 3D space, with a thickness of 20 mm. that used for a 3D printer.

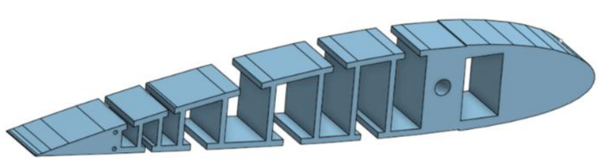
Fig. 4 3D modeling for the printer of the morphing section

Then, by using a 3D printer, the Creality3D CR-X, and PLA material, the resulting molding section is shown in Figure 5.


Fig. 5 3D printed models

A variety of modified wing shapes can be created by varying the angle of the airfoil flap, either upward or downward. This design allows for the extension of the upper and lower airfoil surfaces while maintaining a constant thickness at any curvature. Furthermore, this design is free of design complexities that might complicate its manufacturing process. Moreover, its manufacture using inexpensive raw materials makes it suitable for UAVs. It was observed that the rectangular voids and slots in this corrugated shape significantly affect its bendability. The larger the void, the more difficult to bend, due to the material's inelasticity. Bending depends on the rectangular voids and slots in the airfoil surface. Therefore, increasing these voids in the airfoil provides high bending flexibility without relying entirely on the wing material.

There is no general rule for partitioning; simply identifying the areas where the curvature is greater with larger partitions. So, the spaces were partitioned using the cosine function, where the partition in the middle is large in space, while the trailing edge area is small for more rigidness.

The airfoil recurve system can be used in corrugated wing models where part of the wing is continuous, and the rest is rigid. However, this may not be accurate due to the absence of material effects and FEM calculations. However, it is useful for visualizing such an effect. The method can be summarized by dividing the upper and lower surfaces of the airfoil into multiple points distributed over its contour surface. The points on the surface between the starting and ending of the rectangular corrugated section are calculated for the deflection angle of the morphing airfoil, as shown in Figure 6. The airfoil thickness distribution from the leading edge to the trailing edge of the airfoil is also calculated. The airfoil camber line of the original shape is used to rotate the airfoil coordinate points about the point of rotation inside the airfoil. However, the upper and lower surfaces of the modified airfoil must be adjusted so that each point on the surface rotates by an angle evaluated by multiplying the panel angle by the ratio of the point's distance to its maximum distance. As shown in Figure 7, the airfoil is transformed with a flap angle of 20° or -20°, and the starting point of the corrugated shape or rotation point is (0.3*C, 0), and the ending point is (0.85*C, 0), where the wing chord length is given in Table 1. The equations used for this transformation are given below, and a simple MATLAB code has been written to simulate the modified wing shape.

$$D_n = \sqrt{((x_n - x_c)^2 + (y_n - y_c)^2)}\,, \tag{1}$$

$$D_{max} = \max(D_n)\,, \tag{2}$$

$$\theta_n = \alpha_f * \frac{D_n}{D_{max}}\,, \tag{3}$$

$$\begin{matrix} x_t \\ y_t \end{matrix} = \begin{bmatrix} \cos(\theta_n) & -\sin(\theta_n) \\ \sin(\theta_n) & \cos(\theta_n) \end{bmatrix} \begin{bmatrix} x_n - x_c \\ y_n - y_c \end{bmatrix} + \begin{bmatrix} x_c \\ y_c \end{bmatrix} \tag{4}$$

where n= 1,2,3,...,n, (x_c, y_c) hinge point for morphing airfoil, (x_n, y_n), (x_t, y_t) points were transformed by rotating the surface points, surface points, α_f flap angle.

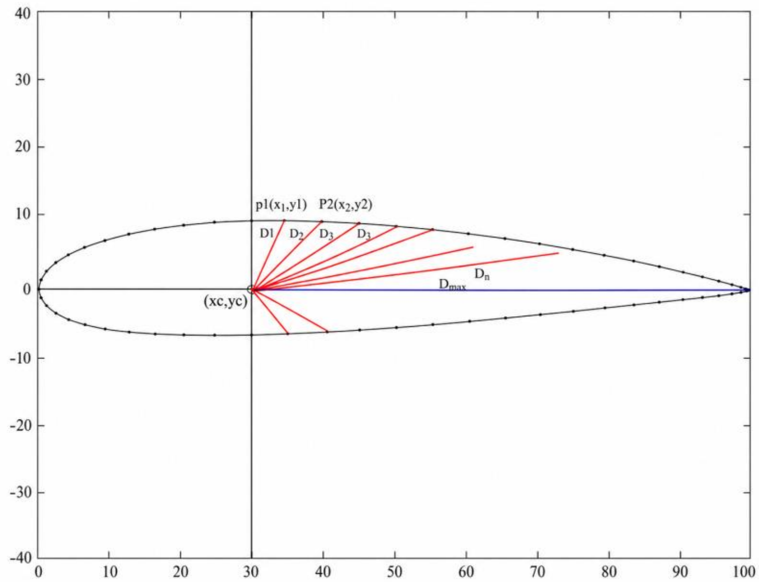

Fig. 6 The original airfoil, hinge point, surface points and surface point distances

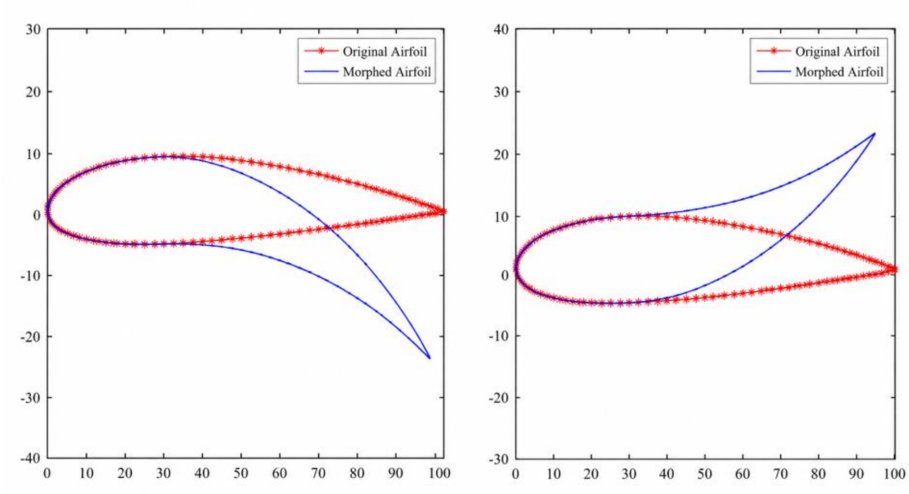

(a) **(b)**

Fig. 7 The original NACA 2415 airfoil and the morphed airfoil with flap, (a) 20˚, and (b) -20 deflections.

Figure 8 shows the morphed airfoil at different angles of flap, which may be introduced as the angle of a straight line connecting the hinge point to the trailing edge, before and after morphing the airfoil (positive or negative). This method enables the shape of the modified airfoil to be estimated in both flap directions, at up and down angles. By matching the rectangular corrugated method with the 3D printed morphed airfoil section, as in Figure 9, the convergence shapes were observed between airfoils. Therefore, the recurve system method can be used to input the modified shapes in the present work into computational programs to calculate the aerodynamic characteristics.

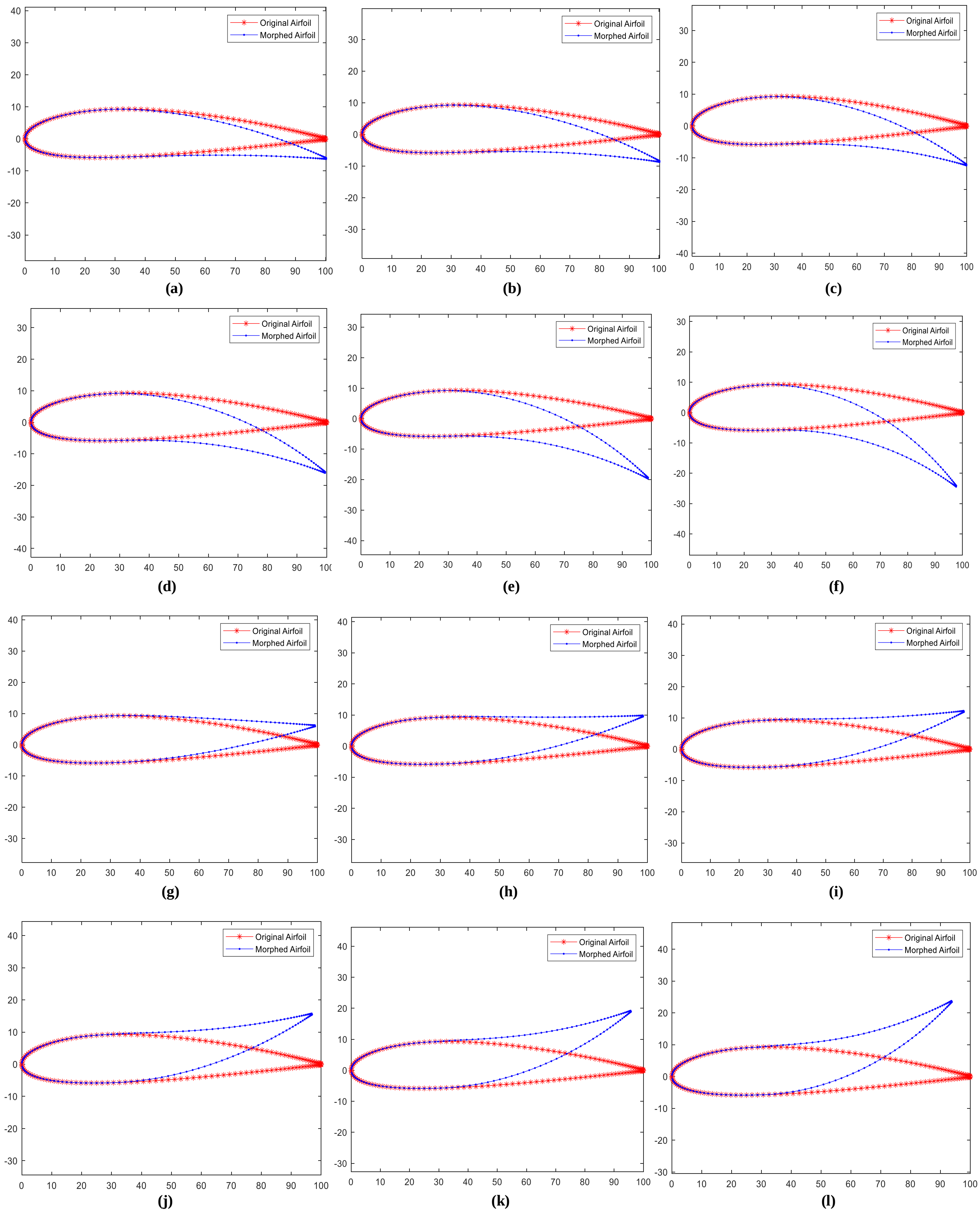

Fig. 8 Morphed airfoil with flap angles is: (a) 5º, (b) 8º, (c) 10º, (d) 12º, (e) 16º, (f) 20º, (g) -5º, (h) -8º, (i) -10º, (j) -12º, (k) -16º, and (l) -20º.

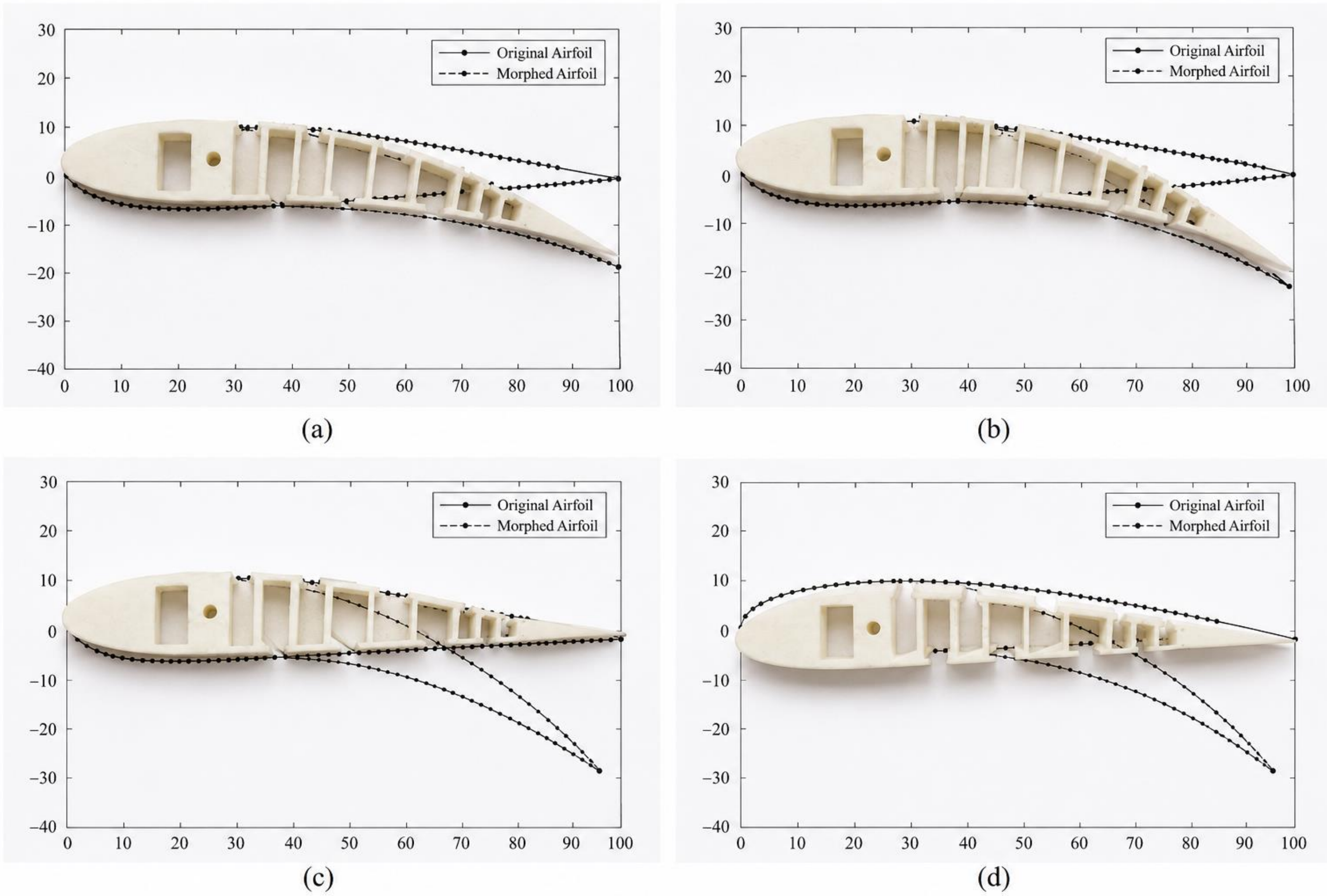

Fig. 9 Matching between 3D printed Morphed airfoil with analytical recurve system method (a) 15˚, (b) 20˚, and (c, d) Original upper and lower surfaces

3. Aerodynamic Analysis

Two methods will be discussed for analyzing and calculating the aerodynamic factors of morphing airfoils. The first method, commonly used and providing rapid results, and the one most researchers in this field have employed, is the viscous-inviscid interaction method. The second method utilizes numerical fluid dynamics, and its details will be presented in the following two sections.

3.1. Viscous-Inviscid Interaction Method (Xflare5 v6)

The aerodynamic characteristics such as lift, drag coefficients, aerodynamic efficiency and pressure distribution of the NACA 2415 wing section will be calculated using the panel method, along with viscous boundary layer calculations using and Xflr5 version 6 [10]. The program calculates the viscous-inviscid interaction flow around the morphing airfoil. This is done by dividing the airfoil surface into several flat panels distributed over the airfoil surface with a linear singularity distribution of source and vortex panels. This method allows for handling many complex shapes involving complex configurations. The method can calculate aerodynamic parameters without the effects of viscosity. Therefore, given the importance of including viscous flow effects in the calculations, by solving boundary layer equations (laminar, transitional, and turbulent flow) to calculate the boundary layer growth on the upper and lower surfaces of the airfoil. The blowing velocity is used to represent the boundary layer displacement on the airfoil surface. The calculations are combined with the estimation of the wake behind the section to evaluate the extension of the boundary layer behind the airfoil. This method is the simplest and can treat multi configuration in a quick process with an acceptable accuracy. All the information for this method is contained in [10], which relates to the program method.

For the geometry, equations 1, 2, 3, and 4 in the previous section are used to generate the morphing airfoil shape. The points representing the airfoil surface are then exported, with the number of points, N = 200. These points are then imported by Xflr5 to be prepared for solving the problem to find the aerodynamic characteristics. The Re is set to 0.688 x 10^6, which corresponds to a speed of 50 m/s for a 200mm airfoil chord, which is a medium speed for a small fixed-wing UAV. This region of flight strikes a balance between aerodynamic performance, controllability, and structural analysis, which may be used for mapping, surveillance, and UAV investigation. The range of angles of attack from 0˚ to 20˚ for all airfoil shapes is illustrated in Figure 8. The Table 2 below shows the information on the cases and settings that will be studied in this work.

Table 2. Airfoil cases and code parameters

Airfoil parameters	Limits
Morphing angle	0-20^o
Angle of attack	0-20^o
Reynolds Number	0.688 x 10^6
Number of panels	200
Free transition ((e^n - method)) Ncrit	9
Max. Number of Iterations	500
Convergence limit	1x10^{-6}

3.2. Computational Fluid Dynamics CFD (EasyCFD v4)

The computational fluid dynamics analysis was calculated by the EasyCFD v4 program [11], which has been used for the numerical simulation of two-dimensional and 3D axisymmetric fluid flow in a boundary-fitted mesh around the morphed airfoil.

Steady state subsonic incompressible flow had been set with the κ-ω SST turbulence model to treat the turbulent flow around the normal and morphing airfoil cases [14, 15]. The 2nd order upwind scheme had been used for the advection differencing scheme.

Figure 10 briefly illustrates the steps for modeling morphing airfoils, where the software provides a simple and systematic environment for modeling two-dimensional shapes by creating a flow field around the airfoil with boundary conditions representing air entering at a constant speed and exiting at a constant pressure, with a similarity boundary condition for distant boundaries.

The figure also illustrates the mesh around the airfoil using rectangular elements, where the domain was divided into approximately 1.6x10^6. The other parameters were arranged in the program to arrive at the final solution and ensure accuracy in the results.

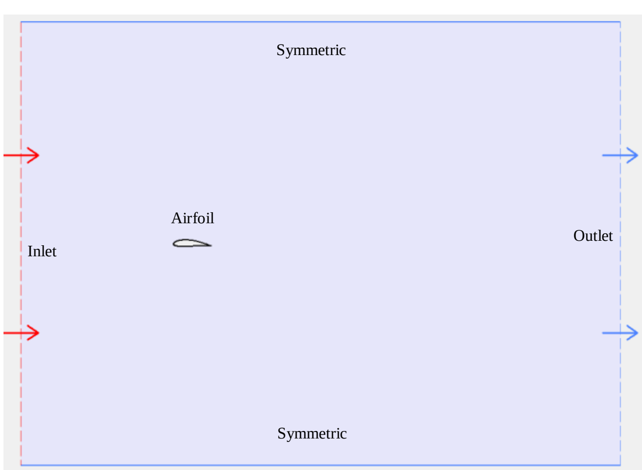

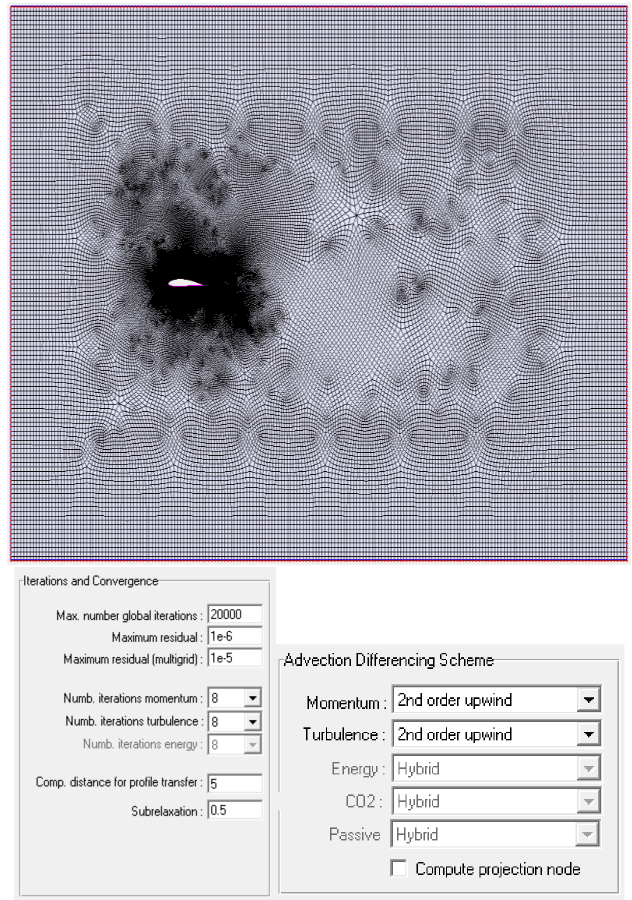

Fig. 10 EasyCFD v4 program setting up to solve the morphing airfoil

4. Numerical Results

4.1. Verification Results

As previously mentioned, to provide confidence in the results obtained from the Xflr5 and EasyCFD programs, which will be used to calculate the RCDC morphing airfoil. As we can see from Figure 11, the convergence of the final solution for the morphing airfoil with an angle of attack of 4^o is shown, and the figure indicates that all lines are less than accuracy 1x10^{-6}.

A comparison was made in Figure 12 for the Xflr5 results, EasyCFD results, CFD solution by Moutaz et al. [12], and the experimental data from James F. [13] at Re=1x10^6 for the normal airfoil shape. The results show an excellent match for lift and lift-to-drag ratio. A small discrepancy between the current results using Xflr5 v6 and the experimental data can be attributed to the simplified mathematical model with the viscous-inviscid interaction method to represent the aerodynamic characteristics.

The overall error percentage of the lift coefficient and the lift-to-drag ratio are 8% and 6%, respectively. The computational fluid dynamics solution by the EasyCFD program confirms the results previously discussed with acceptable differences of about 10% and 3%, respectively.

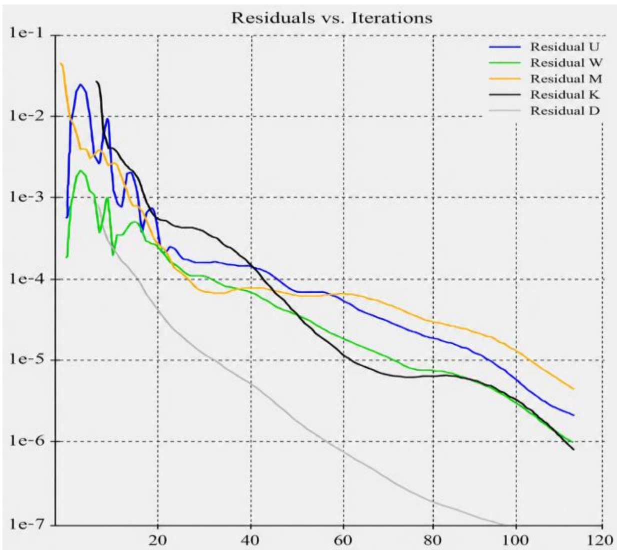

Fig. 11 EasyCFD v4 program the solution convergence for the morphing wing at *α*=4º

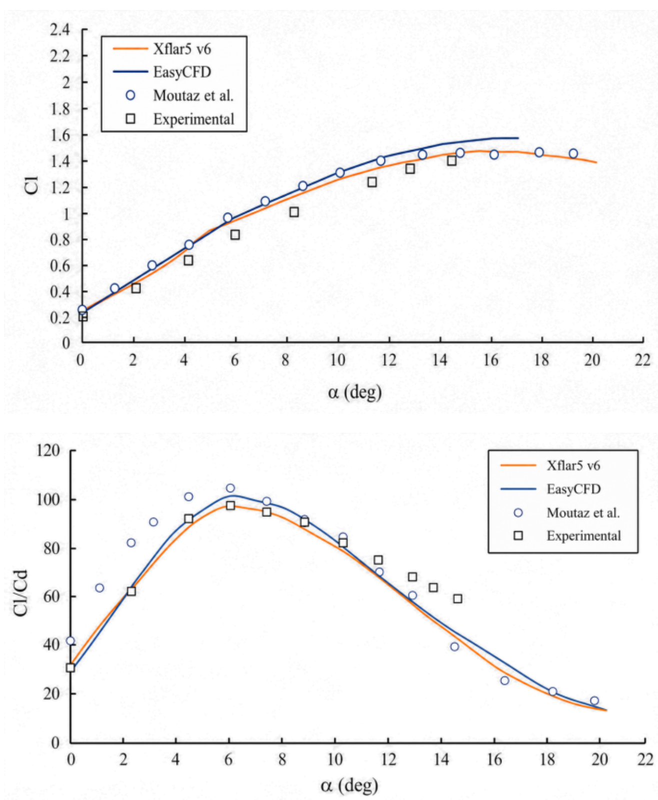

Fig. 12 Comparison between computational and experimental lift and lift-to-drag ratio results for the normal airfoil

This section presents the results of the RCDC morphing airfoil, which is compared with the normal NACA 2415 airfoil and the airfoil with the conventional deflected flap. The results include lift and drag coefficients, as well as the lift-to-drag ratio (aerodynamic efficiency) and pressure coefficients on the airfoil surface. It is important to note that the deflected flap consists of a flap 40% of the airfoil's chord length, measured from the trailing edge of the airfoil. The morphing airfoil was found to exhibit a clear advantage over both the normal airfoil and the airfoil with the deflected flap. The comparison between the deflected flap and the morphing flap is performed at a zero angle of attack but with varying flap angles from 0° to 20°. The results are performed using Xflr5 v6.

Figure 13 illustrates the lift coefficients for the morphing airfoil, the deflected flap airfoil, and the normal airfoil. The comparison was made between the morphed airfoil and deflected flap airfoil at deflection angles (α_f) ranging from 0° to 20° with an angle of attack of 0°. The normal airfoil angles of attack (α) are varied from 0° to 20°. The figure clearly shows that the improvement in the lift coefficients of the morphing airfoil is significant compared to the others.

It can be seen that the deflected flap airfoil with small deflection angles (0°–10°) has the same lift coefficient as the morphing airfoil and is therefore higher than the normal airfoil. This is because the deflected flap increases the lift on the airfoil as long as the flow is minimally separated from the trailing edge. However, by increasing the deflected flap angle, the separation layer is increased.

The lift coefficient begins to decrease abruptly due to the high separation of the flow from the flap, eventually becoming lower than the lift coefficient of the normal airfoil value. Morphing airfoil, on the other hand, has not encountered this issue because of the direct and smooth connection between the front and back edges of the airfoil, creating a seamless flow, unlike that of the deflected flap airfoil. The increase in lift coefficient for the morphing airfoil is 17% compared to the normal airfoil, and the same percentage for the drag coefficient.

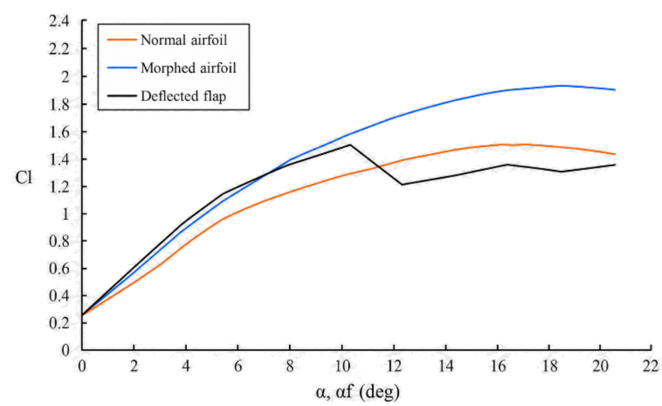

Fig. 13 Lift coefficient comparisons using Xflr5 between NACA 2415 Morphing, normal and deflected flap airfoils

Figure 14 illustrates the drag coefficient for the morphing airfoil, which exhibits a lower airflow separation. For small angles of attack, the drag coefficient of the normal airfoil is lower than that of both the morphing airfoil and deflected flap airfoil. However, due to the increased separation area from the airfoil surface and its flap, the drag coefficients of the normal and deflected flap airfoils are increased while the morphing airfoil is decreased, particularly at high angles. It is observed that for the deflected flap airfoil at low angles (0º-10°), the drag coefficient is similar to that of the morphing airfoil. At high-angle airfoils, drag increases due to the separation of the flow from the airfoil surface, thus increasing the adverse pressure gradient, trying to decrease the momentum of the flow. Morphed airfoils demonstrate superior drag compared to other normal and flapped airfoils. The morphed airfoil has a streamlined shape that minimizes the adverse pressure gradient, thereby preventing the aggravation of the drag force.

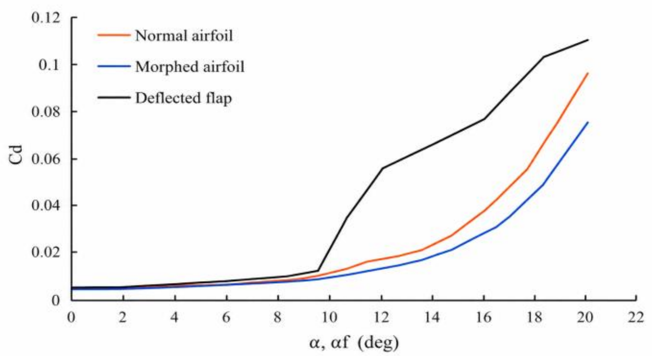

Fig. 14 Drag coefficient comparisons using Xflr5 between NACA 2415 Morphing, normal and deflected flap airfoils

As previously mentioned, all indicator points for the current airfoil's superiority over the deflected flap and normal ones are in terms of lift and drag coefficients. The aerodynamic efficiency is an important indicator of the effectiveness of the current airfoil geometry improvement.

As shown in Figure 15, the maximum value of this ratio and the angle of attack at which it occurs are increased. Similarly, the aerodynamic performance behaves as lift and drag coefficients for the same reasons, which were discussed previously. The increase in aerodynamic efficiency reaches 28% compared to the normal airfoil.

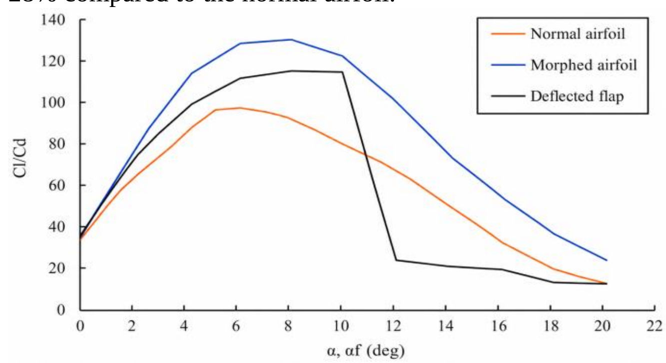

Fig. 15 Lift-to-drag ratio coefficient comparisons using Xflr5 between NACA 2415 Morphing, normal and deflected flap airfoils.

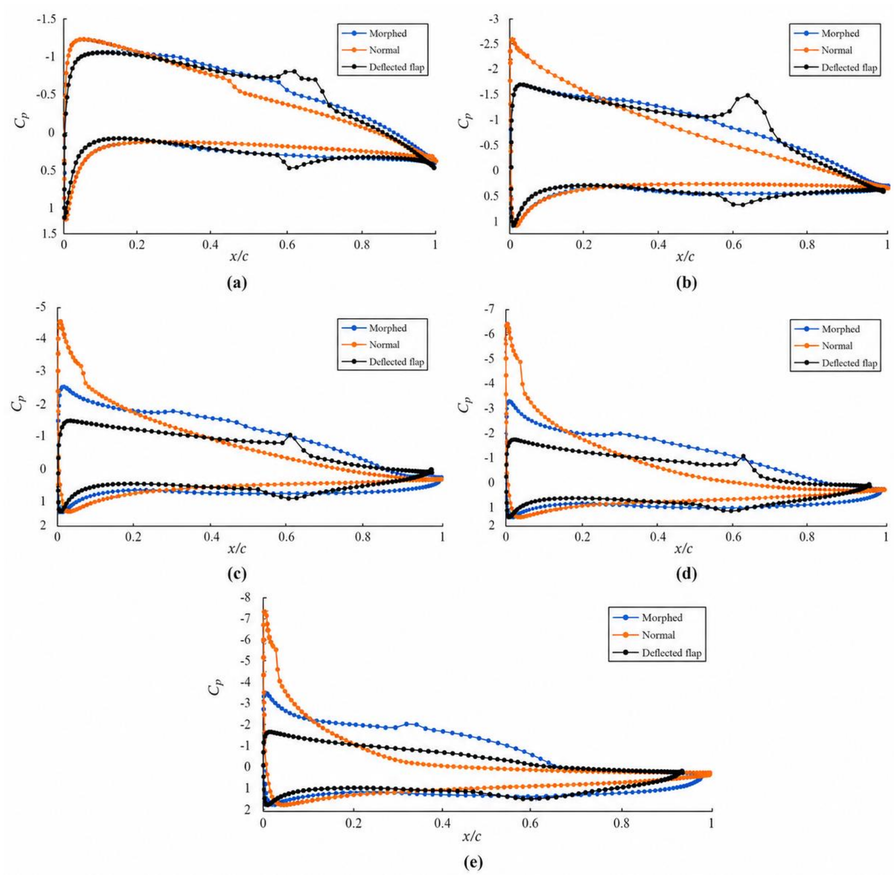

Fig. 16 Cp vs x/c comparisons between NACA 2415 Morphing airfoil, airfoil with deflected flap and original airfoil, (a) 4º, (b) 8˚, (c) 12˚, (d) 16˚, and (e) 20˚.

Figure 16 shows the pressure distributions on the top and bottom surfaces of the morphing airfoil, airfoil with deflected flap, and the normal airfoil for angles 4°, 8°, 12°, 16°, and 20°. In all figures, as a result, show that for the morphing airfoil, which is at the angle of attack of 0°, the pressure coefficient distribution on the top surface is lower than that of the normal airfoil. The airfoil nose region of the morphing airfoil with a deflected flap does not have a suction vortex (representing a region of high negative pressure) because the angle of attack remains zero, unlike the normal airfoil, which exhibits this phenomenon due to increasing angles of attack. This substantial decrease in pressure value results in a high adverse pressure gradient behind it, acting against the flow and thus increasing the separation region behind the original airfoil. As for the lower surface of the airfoil, the pressure coefficient is higher than the normal airfoil pressure, which increases the lift as expected due to the decrease in pressure at the top and the increase in pressure at the bottom. From the trailing edge of the airfoil, a separation region is clear for all types, with a larger one in the normal airfoil than in the morphing one. This can be identified by observing the region where the pressure is of constant values. Therefore, the morphing airfoil offers the advantage of a smaller separation region because its adverse pressure gradient is less pronounced compared to the normal airfoil. The deflected flap airfoil shows a compatible distribution with the morphing airfoil, except in the region of the hinged flap, where a sudden increase and decrease in pressure had been noticed for small angles of deflection (0°-10°). The pressure coefficient for the higher angles had been decreased for the upper surface, and approximately constant distribution for the remaining angles.

Figure 17 illustrates the velocity distribution using the EasyCFD program with turbulent flow and κ-ω SST turbulence model around the variable-camber morphing airfoil at deflection angles of 8º, 12º, 14º, and 16º. Increasing the airfoil's curvature angle leads to an increase in the separation region at the trailing edge. The blue area represents the vortices that are created due to the separation of flow behind the airfoil, which increases the wake thickness behind it. This, in turn, increases drag and reduces lift forces. The scale gradients for all figures are standardized to ensure consistent color rendering and accurately depict the airflow around the wing.

Figure 18 shows the separated area behind the airfoil at a deflection angle of 12º. The vortices associated with the separation of the flow from the airfoil surface are shown using streamline and velocity vectors representation, which result from an increase in the back pressure gradient with friction, and this reduces the flow momentum on the airfoil surface.

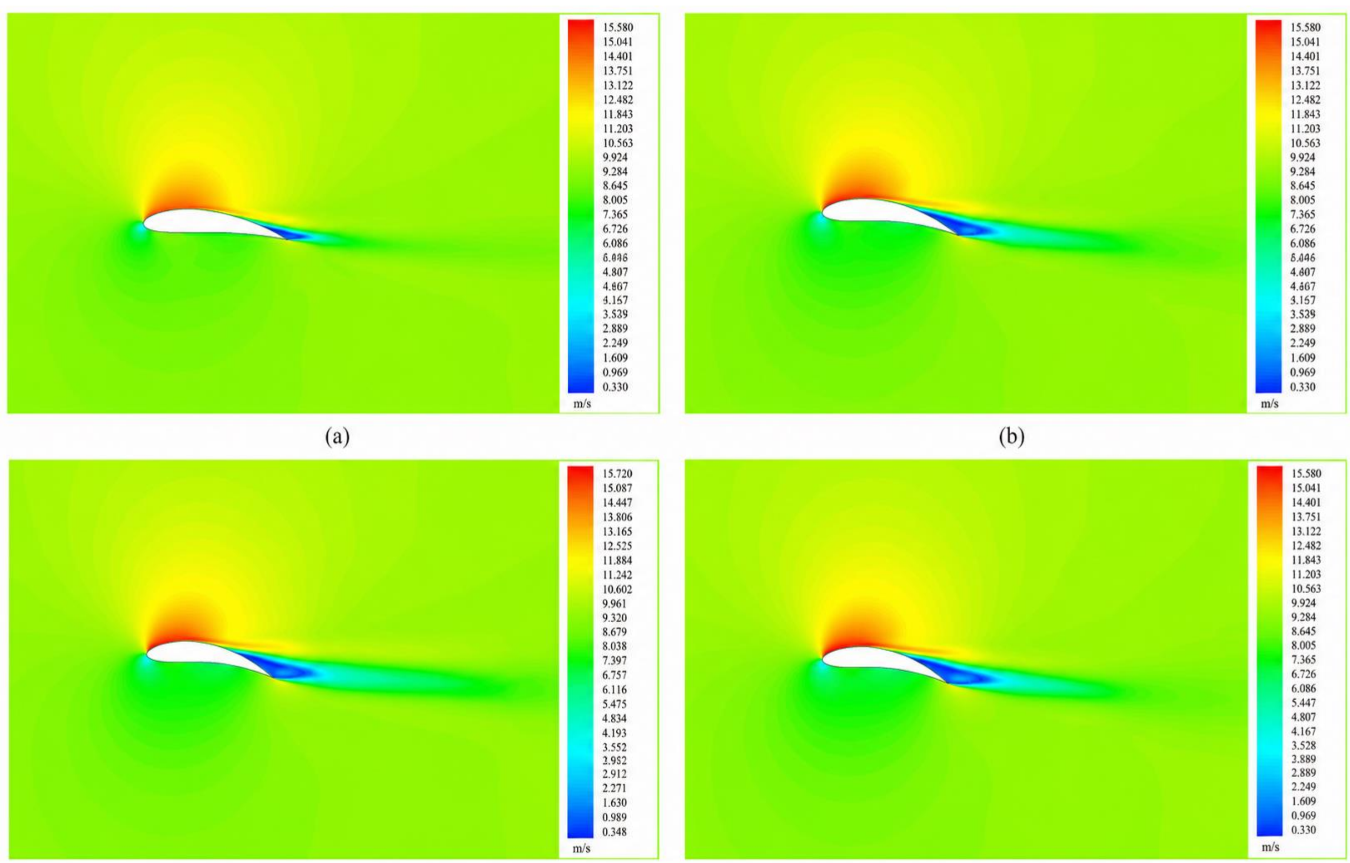

Fig. 17 Velocity distribution of NACA 2415 Morphing airfoil, for deflection angles, (a) 8º, (b) 12º, (c) 14º, and (d) 16º

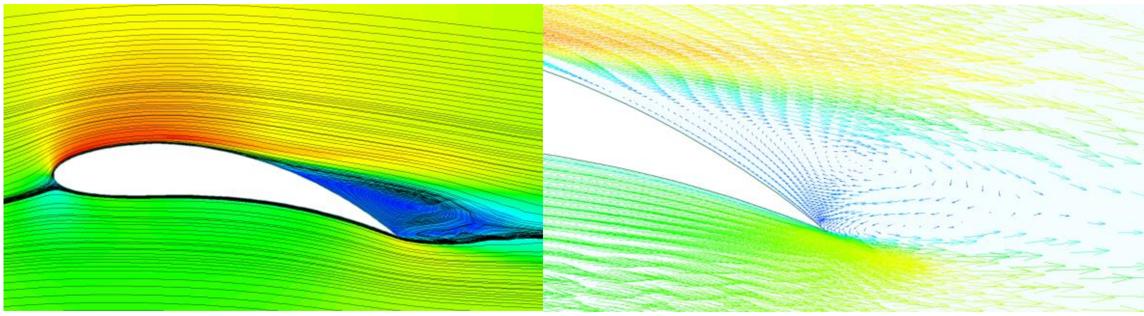

Fig. 18 Streamline and velocity vector of NACA 2415 Morphing airfoil, at deflection angle 14º.

Figure 19 illustrates a comparison of the lift and drag coefficients at a 4° deflection angle between a morphing airfoil and a deflected-flap airfoil for the range of angles of attack (0º-20º). The morphing airfoil clearly outperforms the deflected-flap airfoil. This relates to the previously discussed factors affecting wing performance.

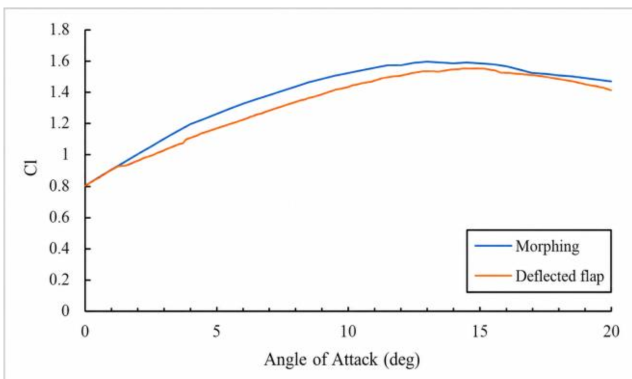

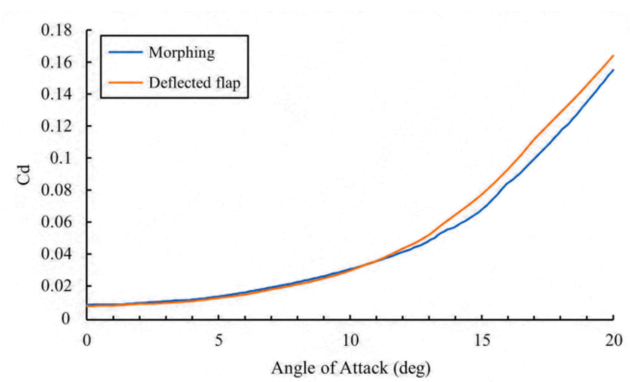

Fig. 19 Lift and Drag coefficients for Morphing airfoil, Deflected Flap Airfoil at deflected angle 4º

In the following Figure 20, each morphing airfoil model was tested for angles of attack from 0 ˚ to 20 ˚, and compared to the original airfoil. It is clear that the improved airfoil geometry significantly increased all of these parameters as compared to the original airfoil. Furthermore, the increased drag coefficient of the morphing airfoil due to early separation of the boundary layer resulted in a decrease in aerodynamic efficiency as angles of attack increased beyond an angle 8º, despite the significant increase in lift coefficient. Cruise flight is often involved, so the improvement is clear, and even at angles of attack up to 8 ˚, there is an improvement in aerodynamic efficiency and coefficients.

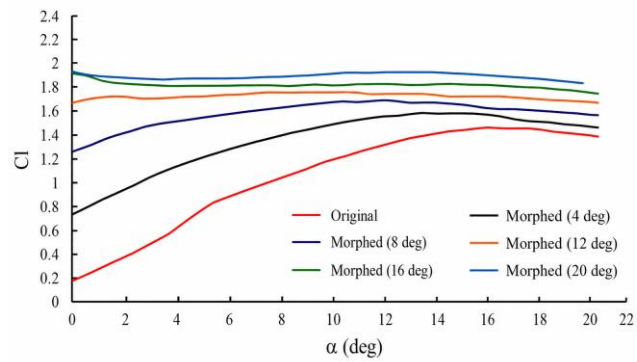

(a)

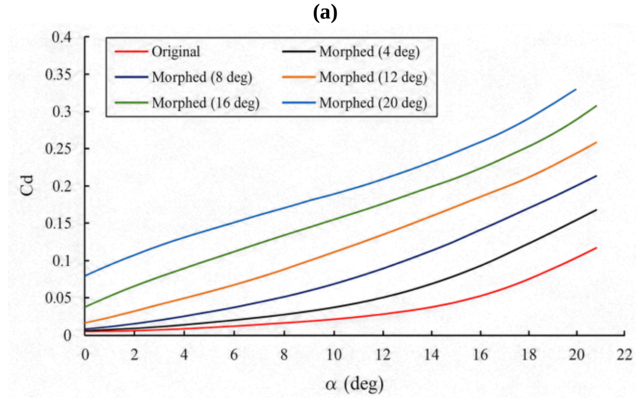

(b)

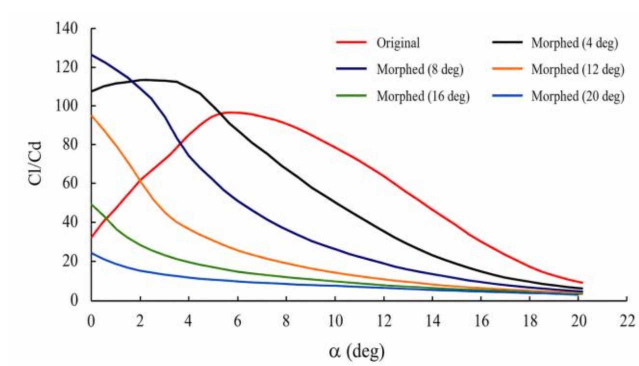

(c)

Fig. 20 Aerodynamic coefficients comparisons between the NACA 2415 Morphing airfoil and original airfoil at different angles of attack

5. Conclusion

In this study, a new design of morphing airfoil configuration using a structure, Rectangular Corrugate Variable Camber (RCVC), was proposed. A comparative study of the present geometry with the normal and traditional deflected flap models for the basis of geometry and aerodynamic analysis is presented. Geometrical approximation of the morphed airfoil is done using simple recurves system equations that are programmed in MATLAB. A 3D printed geometry of the morphed airfoil structure had been compromised with the theoretical geometry. It is found that the RCVC model is more feasible and shows an accurate matching with the MATLAB results. For the aerodynamic analysis, the Xflr5 version 6 was used with the EasyCFD program for computational fluid dynamics for more fidelity of the results. The results of aerodynamic characteristics show that the RCVC model has higher aerodynamic performance. So, from both a geometrical and aerodynamic point of view RCVC model is a feasible and promising morphing wing concept with a percent reach to 28%, increasing in aerodynamic performance.

The proposed morphing mechanism has been physically realized using 3D-printed components, demonstrating its mechanical feasibility. The design is lightweight, low-cost, and suitable for small- to medium-scale UAV applications, making it practical for real-world implementation alongside the aerodynamic advantages presented in this study.

It must be noted that, due to limitations of the present experimental work, the present work does not include repeated experimental measurements, statistical analysis, uncertainty quantification, and error representation.

Future focus will be on implementing the morphing mechanism proposed in the current research, including the operation, control, and real-time synchronization process, as well as real-world testing of experimental aerodynamics under different flight conditions.

Conflicts of Interest

The authors declare that there is no conflict of interest regarding the publication of this paper.

Funding Statement

This research received no external funding.

Acknowledgments

Anmar H. conceived and designed the study, performed the CFD simulations, and developed the proposed correlation for morphed airfoils. Basim A. R. contributed to improving the manuscript by refining the text, expanding the literature review, and adding relevant references. Both authors reviewed and approved the final version of the manuscript.

References

[1] Sha Du, and Haisong Ang, "Design and Feasibility Analyses of Morphing Airfoil Used to Control Flight Attitude," *Journal of Mechanical Engineering*, vol. 58, no. 1, pp. 46-55, 2012. [CrossRef] [Google Scholar] [Publisher Link]

[2] R. Wu et al., "A Morphing Aerofoil with Highly Controllable Aerodynamic Performance," *The Aeronautical Journal*, vol. 121, no. 1235, pp. 54-72, 2017. [CrossRef] [Google Scholar] [Publisher Link]

[3] D. Kumar, S. Faruque Ali, and A. Arockiarajan, "Structural and Aerodynamics Studies on Various Wing Configurations for Morphing," *IFAC-Papers on Line*, vol. 51, no. 1, pp. 498-503, 2018. [CrossRef] [Google Scholar] [Publisher Link]

[4] Urban Fasel et al., "Composite Additive Manufacturing of Morphing Aerospace Structures," *Manufacturing Letters*, vol. 23, pp. 85-88, 2020. [CrossRef] [Google Scholar] [Publisher Link]

[5] Ben Moulton, and Douglas F. Hunsaker, *3D-Printed Wings with Morphing Trailing-Edge Technology*, AIAA Scitech 2021 Forum, 2021. [CrossRef] [Google Scholar] [Publisher Link]

[6] K. Dhileep et al., "Aerodynamic Study of Single Corrugated Variable-Camber Morphing Aerofoil Concept," *The Aeronautical Journal*, vol. 126, no. 1296, pp. 316-344, 2022. [CrossRef] [Google Scholar] [Publisher Link]

[7] Sijia Jia et al., "Wind Tunnel Tests of 3D-Printed Variable Camber Morphing Wing," *Aerospace*, vol. 9, no. 11, pp. 1-26, 2022. [CrossRef] [Google Scholar] [Publisher Link]

[8] Nebojša Lukić et al., "Numerical Investigation and Optimization of a Morphing Airfoil Designed for Lower Reynolds Number," *Aerospace*, vol. 11, no. 4, pp. 1-16, 2024. [CrossRef] [Google Scholar] [Publisher Link]

[9] Reem Aly et al., "Investigation of a Variable Camber Morphing Airfoil via SMA Wire and Corrugated Structures," *International Journal of Aeronautical and Space Sciences*, vol. 26, pp. 562-577, 2025. [CrossRef] [Google Scholar] [Publisher Link]

[10] XFLR5, Flow5, 2026. [Online]. Available: https://www.flow5.tech/xflr5/xflr5.html

[11] Numerical Calculation of Fluid Flow and Heat Transfer in 2D and 3D Axisymmetric Domains, EasyCFD. [Online]. Available: https://www.easycfd.net/

[12] Moutaz Elgammi, Aljonid Aokaly, and Yasser Aldali, "Development of a New Airfoil Profile with a High Lift-to-Drag Ratio for Wind Turbines using a Low Fidelity Accurate Optimization Flow Solver," *Energy Harvesting and Systems*, vol. 8, no. 1, pp. 13-27, 2021. [CrossRef] [Google Scholar] [Publisher Link]

[13] James F. Marchman, *Aerodynamics and Aircraft Performance*, 3rd ed., Virginia Tech, 2004. [Google Scholar] [Publisher Link]

[14] Ahmed Tawfeeq Mustafa Ali ABED, "Computational Analysis of SD7037 Airfoil with Plain Flap," *Archive of Mechanical Engineering*, vol. 71, no. 4, pp. 561-580, 2024. [CrossRef] [Google Scholar] [Publisher Link]

[15] A.A. Ali, A.A. Hussein, and S.M. Hafedh, "Aerodynamic Analysis of SD7037 Airfoil with Flex-Skin Flap at Low Angles of Attack and Low Reynolds Numbers," *Scientific and Technical Journal of Information Technologies*, *Mechanics and Optics*, vol. 25, no. 6, pp. 1208-1219, 2025. [CrossRef] [Google Scholar] [Publisher Link]